

Formation of atomically ordered and chemically selective Si—O—Ti monolayer on Si_{0.5}Ge_{0.5}(110) for a MIS structure via H₂O₂(g) functionalization

Sang Wook Park,¹ Jong Youn Choi,¹ Shariq Siddiqui,² Bhagawan Sahu,² Rohit Galatage,² Naomi Yoshida,³ Jessica Kachian,³ and Andrew C. Kummel^{1,4,a)}

¹Materials Science and Engineering Program, University of California, La Jolla, San Diego, California 92093, USA

²TD Research, GlobalFoundries USA Inc., 257 Fuller Road, Albany, New York 12203, USA

³Applied Materials, Inc., Santa Clara, California 95054, USA

⁴Department of Chemistry and Biochemistry, University of California, La Jolla, San Diego, California 92093, USA

(Received 11 July 2016; accepted 19 October 2016; published online 14 November 2016)

Si_{0.5}Ge_{0.5}(110) surfaces were passivated and functionalized using atomic H, hydrogen peroxide (H₂O₂), and either tetrakis(dimethylamino)titanium (TDMAT) or titanium tetrachloride (TiCl₄) and studied *in situ* with multiple spectroscopic techniques. To passivate the dangling bonds, atomic H and H₂O₂(g) were utilized and scanning tunneling spectroscopy (STS) demonstrated unpinning of the surface Fermi level. The H₂O₂(g) could also be used to functionalize the surface for metal atomic layer deposition. After subsequent TDMAT or TiCl₄ dosing followed by a post-deposition annealing, scanning tunneling microscopy demonstrated that a thermally stable and well-ordered monolayer of TiO_x was deposited on Si_{0.5}Ge_{0.5}(110), and X-ray photoelectron spectroscopy verified that the interfaces only contained Si—O—Ti bonds and a complete absence of GeO_x. STS measurements confirmed a TiO_x monolayer without mid-gap and conduction band edge states, which should be an ideal ultrathin insulating layer in a metal-insulator-semiconductor structure. Regardless of the Ti precursors, the final Ti density and electronic structure were identical since the Ti bonding is limited by the high coordination of Ti to O. *Published by AIP Publishing.* [<http://dx.doi.org/10.1063/1.4966690>]

I. INTRODUCTION

As the size of Si-based complimentary metal-oxide semiconductor (CMOS) devices decreases, new materials have been developed to enhance device performance. Silicon-germanium (SiGe) has received much attention due to its applications in strain engineering and higher mobility.^{1–3} The larger lattice constant of SiGe has been utilized in n-type MOS transistors to improve electron mobility by applying a biaxial tensile stress into Si channels.^{4,5} Alternatively, when SiGe materials were employed in the source or drain areas, a compressive stress was utilized for the enhancement of hole mobility in p-type MOS transistors.^{6,7} Furthermore, due to the higher mobility of SiGe compared to silicon, SiGe has been employed as a channel material in p-type MOS transistors.⁸ However, to utilize SiGe in the source and drain in very large scale integrated (VLSI) technology, source/drain resistance must be minimized.⁹

While few studies have looked at passivation of SiGe as a contact material, many studies have reported passivation of SiGe and Ge as channel materials. Extensive studies have been reported to passivate the channel surfaces with low interface state density (D_{it}) and unpinned Fermi level. Passivation of Ge via ozone oxidation below 400 °C resulted

in low D_{it} by suppressing the formation of Ge suboxide in favor of GeO₂.¹⁰ Lee *et al.*¹¹ demonstrated that water (H₂O) was effective in passivating Ge(001) surfaces as verified by scanning tunneling microscopy (STM) and scanning tunneling spectroscopy (STS) measurements. Recent studies verified that hydrogen peroxide vapor (H₂O₂(g)) formed a more stable passivation layer and a higher nucleation density for atomic layer deposition (ALD) than H₂O(g) on Ge(001),¹² SiGe(001),¹³ and SiGe(110)¹⁴ surfaces, thereby improving the formation of high-k dielectrics.

Extremely thin insulator interfaces have been used to form unpinned contacts on Ge and SiGe substrates. Kobayashi *et al.*¹⁵ deposited an ultrathin tunnel barrier of Si₃N₄ between the contact metal and a Ge substrate to form a metal-insulator-semiconductor (MIS) structure. However, the insulating layer of Si₃N₄ introduced a large tunneling resistance due to the significant conduction band offset (CBO) to the Ge substrate. Lieten *et al.*¹⁶ formed a thin Ge₃N₄ layer on Ge substrates for ohmic contacts, and this layer passivated Ge surface states. Lin *et al.*¹⁷ employed a 7.1 nm-thick TiO₂ interfacial layer in a MIS structure to reduce the tunneling resistance by having nearly zero CBO. The TiO₂ films deposited on SiGe(001) for MIS capacitors minimized D_{it} as demonstrated by capacitance-voltage and conductance-voltage measurements.¹⁸

In this report, the topological, electronic, and chemical properties of Si_{0.5}Ge_{0.5}(110) were studied for the application as a MIS structure. Exposure of atomic H or H₂O₂(g) passiv-

a) Author to whom correspondence should be addressed. Electronic mail: akummel@ucsd.edu.

ated the dangling bonds on sputter-cleaned $\text{Si}_{0.5}\text{Ge}_{0.5}(110)$ with hydrogen atoms or hydroxyl groups resulting in an unpinned Fermi level. $\text{H}_2\text{O}_2(\text{g})$ also was utilized to form a high density of OH sites which is advantageous for the formation of a high density ultrathin insulating layer in a MIS structure. Subsequent tetrakis(dimethylamino)titanium (TDMAT) or titanium tetrachloride (TiCl_4) dosing via ALD functionalized the hydroxyl-terminated $\text{Si}_{0.5}\text{Ge}_{0.5}(110)$ with Ti atoms, thereby forming a monolayer of TiO_x on $\text{Si}_{0.5}\text{Ge}_{0.5}(110)$ surfaces. Annealing studies demonstrated the thermal and electronic stability of a TiO_x monolayer on $\text{Si}_{0.5}\text{Ge}_{0.5}(110)$ surfaces and the complete absence of GeO_x at the interface; instead the interface was composed solely of Si—O—Ti bonds. Each experimental process was probed using *in situ* STM, STS, and X-ray photoelectron spectroscopy (XPS).

II. EXPERIMENTAL

P-type $\text{Si}_{0.5}\text{Ge}_{0.5}(110)$ films with 10^{15} cm^{-3} B doping grown on Si(110) wafers were provided by GLOBAL-FOUNDRIES and diced into $10.5 \times 5.5 \text{ mm}^2$ pieces. Each sample was repeatedly cleaned via a degreasing method using acetone, methanol, and deionized water then dried with N_2 gas. Samples were loaded into a customized Omicron ultra-high vacuum (UHV) preparation chamber with a base pressure of 1×10^{-10} Torr and prepared by combined sputtering and annealing processes. The sputtering process utilized a 1.5 kV argon ion (Ar^+) beam (Model 1403 ion gun, Nonsequitur Technologies) with a current of $0.9 \mu\text{A}$ and an Ar gas pressure of 6×10^{-7} Torr for 30 min, while the sample temperature was maintained at $500 \text{ }^\circ\text{C}$ using resistive pyrolytic boron nitride (PBN) heating. An annealing process was performed at a sample temperature of $500 \text{ }^\circ\text{C}$ for 30 min. After repeated sputter and annealing cycles, the chemical, topological, and electronic characteristics were studied via *in situ* XPS, STM, and STS.

Sputter-cleaned $\text{Si}_{0.5}\text{Ge}_{0.5}(110)$ samples were reacted with atomic hydrogen in the UHV preparation chamber using a thermal gas cracker (Atomic Hydrogen Source, Veeco). The gas pressure was controlled via a leak valve and measured with an ion gauge; the exposure was calculated in terms of Langmuirs ($1 \text{ Langmuir (L)} = 1 \times 10^{-6} \text{ Torr s}$). During the atomic hydrogen dose, the temperature of filament was maintained between 1800 and $2200 \text{ }^\circ\text{C}$, while the temperature of $\text{Si}_{0.5}\text{Ge}_{0.5}(110)$ samples was maintained at $300 \text{ }^\circ\text{C}$; the cracking efficiency was expected to be 30%, but the reported amount of atomic H dose was estimated based solely on the H_2 pressure, so the actual amount of atomic H dose should be smaller compared to the reported value. During the experiment, H_2 was dosed at 1×10^{-5} Torr for 360 s; this is reported below as 3600 L of atomic H.

To avoid air exposure, samples were transferred to an *in situ* ALD chamber with a base pressure of 1×10^{-7} Torr. $\text{H}_2\text{O}_2(\text{g})$, TDMAT, and TiCl_4 were dosed at $25 \text{ }^\circ\text{C}$ surface temperature by filling the dosing chamber at $25 \text{ }^\circ\text{C}$ without a carrier gas. As a control experiment, $\text{Si}_{0.5}\text{Ge}_{0.5}(110)$ samples were also dosed with $\text{H}_2\text{O}(\text{g})$ at $25 \text{ }^\circ\text{C}$. To achieve

saturated nucleation on $\text{Si}_{0.5}\text{Ge}_{0.5}(110)$ surfaces, a 30% solution of $\text{H}_2\text{O}_2(\text{aq})$ (Fisher Scientific), TDMAT (99%, Strem Chemicals), and TiCl_4 (99%, Strem Chemicals) were utilized. In this paper, the " $\text{H}_2\text{O}_2(\text{g})$ " refers to the mixture of $\text{H}_2\text{O}_2(\text{g})/\text{H}_2\text{O}(\text{g})$; the $\text{H}_2\text{O}_2(\text{aq})$ solution was composed of both components and the $\text{H}_2\text{O}_2(\text{g})$ reaction should be dominant due to its high reactivity. Based on a previous report, a 30% solution of $\text{H}_2\text{O}_2(\text{aq})$ resulted in a vapor of 2.67% $\text{H}_2\text{O}_2(\text{g})$ at $25 \text{ }^\circ\text{C}$;¹⁹ therefore, the actual amount of $\text{H}_2\text{O}_2(\text{g})$ involved in the chemical reaction should be smaller than the reported amount of total vapor below. During the experiment, $\text{H}_2\text{O}_2(\text{aq})$ was dosed at 30 mTorr for 150 s to provide 4.5×10^6 L of total vapor from $\text{H}_2\text{O}_2(\text{aq})$; the maximum amount of $\text{H}_2\text{O}_2(\text{g})$ should be 120 000 L. Before the samples were transferred to the ALD chamber, the chamber was baked overnight by heating the chamber walls to $120 \text{ }^\circ\text{C}$ to minimize the background O and H_2O contaminations. In addition, several cycles of $\text{H}_2\text{O}_2(\text{g})$, TDMAT, and TiCl_4 were pre-dosed to minimize the chemical reaction with the stainless-steel chamber walls during the actual experiments.

Chemical properties from each experimental step were studied with an *in situ* monochromatic XPS (XM 1000 MkII/SPHERA, Omicron Nanotechnology). For the XPS studies, an Al $K\alpha$ source (1486.7 eV) was utilized as an anode material; spectra were measured with a constant analyzer-energy (CAE) mode with a pass energy of 50 eV and a step width of 0.1 eV. The take-off angle between the analyzer axis and the sample normal was 60° and the analyzer-acceptance angle was 7° . For peak shape analysis, a CASA XPS v.2.3 program was utilized via a Shirley background subtraction.

The samples were transferred to an *in situ* STM chamber (LT-STM, Omicron Nanotechnology) with a base pressure of 1×10^{-11} Torr to probe the topological and electronic properties on the $\text{Si}_{0.5}\text{Ge}_{0.5}(110)$ surface after each experimental process. Constant-current mode ($I_{\text{sp}} = 200 \text{ pA}$) STM was performed with a sample bias between -2.0 and -1.8 V to obtain filled-state STM images. Variable-z mode STS was performed with a modulation signal ($0.1 \text{ V}_{\text{ac}}$, 650 Hz) through an external lock-in amplifier (SR830 DSP, Stanford Research Systems) to directly obtain the dI/dV along with the I/V spectra while varying the sample bias from -1.5 to $+1.5 \text{ V}$ and simultaneously moving the tip position forward then backward during the scan to increase the sensitivity with regard to small currents.^{20,21} As described in a previous report,^{14,22} the raw I/V data were smoothed through a low-pass filter with energy width of $(3.0 \text{ eV})/2\pi$ (frequency parameter value in filter of $(3.0 \text{ eV})^{-1}$). This smoothing step led to a broadened I/V , denoted as $\overline{(I/V)}$, which forms a suitable normalization quantity for dI/dV .²² For the precise STS measurements, at least 5 individual spectra of $(dI/dV)/\overline{(I/V)}$ were rescaled from 0 to 1 and subsequently averaged into a single spectrum in the STS figures. Since the $(dI/dV)/\overline{(I/V)}$ spectrum has the property that band onsets have a linear dependence on the sample bias, they were fit with a linear function to extract the band edge energies.²² Based on previous STS studies,^{22,23} a fitting method was performed to extract the band edge energies for the $(dI/dV)/\overline{(I/V)}$ spectra using

a linear function depending on both operational temperature and alternating current (AC) modulation. The calculated linear fits for each STS measurement were included as the solid lines and the onsets of the linear fits corresponding to the band edge energies were calculated with error ranges. The obtained error ranges from the fitting method were standard errors of the least-squares fits and did not reflect thermal broadening nor inaccuracies due to band edge states. Note that the resolution of the bias step from the experimental STS measurements was lower than the extracted error ranges from the linear fits. These results from the linear fits using a very large number of data points; therefore, the small reported error is the uncertainty in the fit to the data and does not reflect systematic errors in the measurements and fittings such as small band tail states and the work function of the tip.

III. RESULTS AND DISCUSSION

To understand the intrinsic surface reactivity, a clean $\text{Si}_{0.5}\text{Ge}_{0.5}(110)$ surface without carbon and oxygen should be prepared. However, several cleaning procedures utilizing aqueous HCl ²⁴ or HF ^{25–27} cleaning left SiGe surfaces with oxygen and carbon contaminations. Conversely, it was demonstrated that a combined sputtering and annealing process produces clean SiGe surfaces without carbon and oxygen.^{13,14} $\text{Si}_{0.5}\text{Ge}_{0.5}(110)$ surfaces were cleaned via several cycles of sputtering with an Ar gas pressure of 6×10^{-7} Torr for 30 min and annealing at 500 °C, and the cleanness of the surfaces was verified by an *in situ* XPS showing no carbon and oxygen at the surfaces. As explained in the [supplementary material](#), a sputter-cleaned $\text{Si}_{0.5}\text{Ge}_{0.5}(110)$ should be terminated with adatoms, which induce a pinned Fermi level due to the half-filled dangling bonds. To form an unpinned Fermi level, 3600 L of atomic H was dosed onto $\text{Si}_{0.5}\text{Ge}_{0.5}(110)$ while the substrate temperature was maintained at 300 °C. Afterwards, sputter-cleaned or atomic H dosed $\text{Si}_{0.5}\text{Ge}_{0.5}(110)$ samples were transferred to an *in situ* ALD chamber to functionalize the surfaces with hydroxyls. For the saturation reaction, 4.5×10^6 L of vapor from $\text{H}_2\text{O}_2(\text{aq})$, which was composed of approximately 120 000 L $\text{H}_2\text{O}_2(\text{g})$ and the balance $\text{H}_2\text{O}(\text{g})$, was dosed onto the samples at 25 °C and this amount was expected to be a saturation dose which would fully react with $\text{Si}_{0.5}\text{Ge}_{0.5}(110)$ surfaces.

To understand the surface reaction after atomic H or $\text{H}_2\text{O}_2(\text{g})$ dosing of $\text{Si}_{0.5}\text{Ge}_{0.5}(110)$ surfaces, schematic models were proposed based on the XPS studies in the [supplementary material](#). XPS data showed that a full saturation dose of $\text{H}_2\text{O}_2(\text{g})$ at 25 °C resulted in an O/(Si + Ge) ratio of 19%, which corresponded to ~ 1.05 monolayers (see Fig. S3 in the [supplementary material](#)). For a 25 °C H_2O_2 dose on H-terminated $\text{Si}_{0.5}\text{Ge}_{0.5}(110)$, the O/(Si + Ge) ratio was identical to 25 °C $\text{H}_2\text{O}_2/\text{Si}_{0.5}\text{Ge}_{0.5}(110)$ demonstrating a strong reactivity of 25 °C $\text{H}_2\text{O}_2(\text{g})$ on H-terminated $\text{Si}_{0.5}\text{Ge}_{0.5}(110)$ to replace H atoms with hydroxyls. In addition, the chemical shifts of Ge— O_xH_y and Si— O_xH_y on 25 °C $\text{H}_2\text{O}_2/\text{Si}_{0.5}\text{Ge}_{0.5}(110)$ and 25 °C $\text{H}_2\text{O}_2/300$ °C atomic H/ $\text{Si}_{0.5}\text{Ge}_{0.5}(110)$ surfaces mainly corresponded to Ge^{2+} and

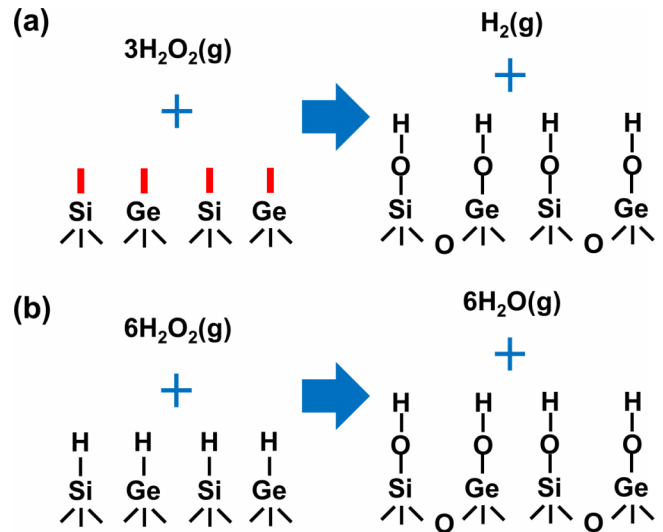


FIG. 1. Proposed models of clean and H-terminated $\text{Si}_{0.5}\text{Ge}_{0.5}(110)$ surfaces dosed with 25 °C $\text{H}_2\text{O}_2(\text{g})$. (a) A schematic diagram of a 25 °C $\text{H}_2\text{O}_2(\text{g})$ dosing of a clean $\text{Si}_{0.5}\text{Ge}_{0.5}(110)$ surface terminated with dangling bonds (red). The surface was terminated with hydroxyls with O insertion into backbonds and the byproduct is $\text{H}_2(\text{g})$. (b) A schematic diagram of a 25 °C $\text{H}_2\text{O}_2(\text{g})$ dose on a H-terminated $\text{Si}_{0.5}\text{Ge}_{0.5}(110)$ surface. $\text{H}_2\text{O}_2(\text{g})$ was sufficiently reactive to form hydroxyl termination at the surface with $\text{H}_2\text{O}(\text{g})$ as a byproduct.

Si^{2+} (see Fig. S5 in the [supplementary material](#)). Fig. 1 presents schematic diagrams for 25 °C $\text{H}_2\text{O}_2(\text{g})$ reactions with clean or H-terminated $\text{Si}_{0.5}\text{Ge}_{0.5}(110)$ surfaces. As shown in Fig 1(a), a saturation $\text{H}_2\text{O}_2(\text{g})$ dose on a clean $\text{Si}_{0.5}\text{Ge}_{0.5}(110)$ surface, which was terminated with half-filled dangling bonds from adatoms, formed hydroxyls on dangling bonds along with oxygen inserted into adatom backbonds with $\text{H}_2(\text{g})$ as a byproduct. Similarly, when a H-terminated $\text{Si}_{0.5}\text{Ge}_{0.5}(110)$ surface was dosed with a saturation $\text{H}_2\text{O}_2(\text{g})$ at 25 °C, $\text{H}_2\text{O}_2(\text{g})$ was sufficiently reactive to replace H atoms with hydroxyls on $\text{Si}_{0.5}\text{Ge}_{0.5}(110)$ and to insert additional oxygen atoms into Si—Ge backbonds, producing $\text{H}_2\text{O}(\text{g})$ as a byproduct as shown in Fig. 1(b). In sum, when a clean or H-terminated $\text{Si}_{0.5}\text{Ge}_{0.5}(110)$ surface was exposed to a saturation dose of $\text{H}_2\text{O}_2(\text{g})$ at 25 °C, the top surface should be terminated with hydroxyls and additional oxygen atoms were likely to break the backbonds resulting in oxygen insertion consistent with

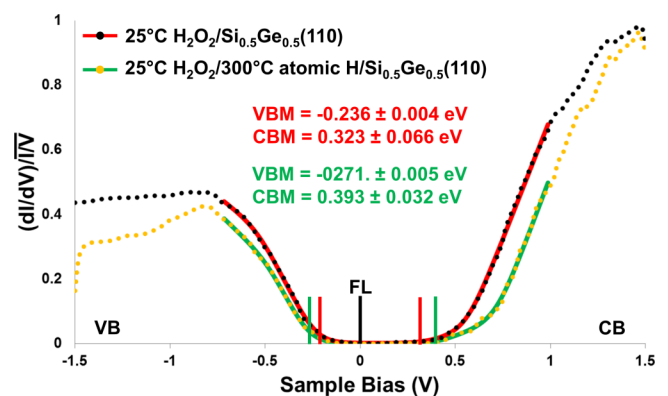


FIG. 2. STS of H_2O_2 dosed $\text{Si}_{0.5}\text{Ge}_{0.5}(110)$ surfaces STS spectra with fits to estimate VB and CB edges. After a 25 °C $\text{H}_2\text{O}_2(\text{g})$ dose, the electronic structures are nearly identical with an unpinned Fermi level regardless of an atomic H dose.

the XPS intensities and chemical shifts corresponding to Ge^{2+} and Si^{2+} in the [supplementary material](#).

The electronic properties of 25 °C $\text{H}_2\text{O}_2/\text{Si}_{0.5}\text{Ge}_{0.5}(110)$ and 25 °C $\text{H}_2\text{O}_2/300$ °C atomic $\text{H}/\text{Si}_{0.5}\text{Ge}_{0.5}(110)$ surfaces were studied through STS measurements in Fig. 2. STS measurements of $(dI/dV)/(I/V)$ are known to be proportional to the local density of states (LDOS);^{21,22} therefore, STS measurements were performed to understand the electronic structures of the surfaces. STS spectra of 25 °C $\text{H}_2\text{O}_2/\text{Si}_{0.5}\text{Ge}_{0.5}(110)$ surface (black) demonstrated the nearly identical electronic structure to 25 °C $\text{H}_2\text{O}_2/300$ °C atomic $\text{H}/\text{Si}_{0.5}\text{Ge}_{0.5}(110)$ surface (yellow) with ± 0.1 V difference with regard to valence band maximum (VBM) and conduction band minimum (CBM), respectively. While the clean p-type $\text{Si}_{0.5}\text{Ge}_{0.5}(110)$ surface had a Fermi level pinned

near mid-gap (as demonstrated in Fig. S2 in the [supplementary material](#)), the Fermi levels of 25 °C $\text{H}_2\text{O}_2/\text{Si}_{0.5}\text{Ge}_{0.5}(110)$ and 25 °C $\text{H}_2\text{O}_2/300$ °C atomic $\text{H}/\text{Si}_{0.5}\text{Ge}_{0.5}(110)$ surfaces were positioned closer to the VB edge consistent with Fermi level unpinning. In addition, the bandgaps were decreased due to the increased density of states near VB and CB edges. Based on STS analysis, it was demonstrated that a 25 °C $\text{H}_2\text{O}_2(\text{g})$ dosing on clean or H terminated $\text{Si}_{0.5}\text{Ge}_{0.5}(110)$ resulted in electronically identical surfaces.

To functionalize the surfaces with Ti atoms for the TiO_x formation, the 25 °C $\text{H}_2\text{O}_2/\text{Si}_{0.5}\text{Ge}_{0.5}(110)$ and 25 °C $\text{H}_2\text{O}_2/300$ °C atomic $\text{H}/\text{Si}_{0.5}\text{Ge}_{0.5}(110)$ surfaces were dosed with 4.5×10^5 L of TDMAT or 4.5×10^5 L of TiCl_4 without carrier gas at 25 °C in an *in situ* ALD chamber. Fig. 3 shows the chemical compositions after a saturation

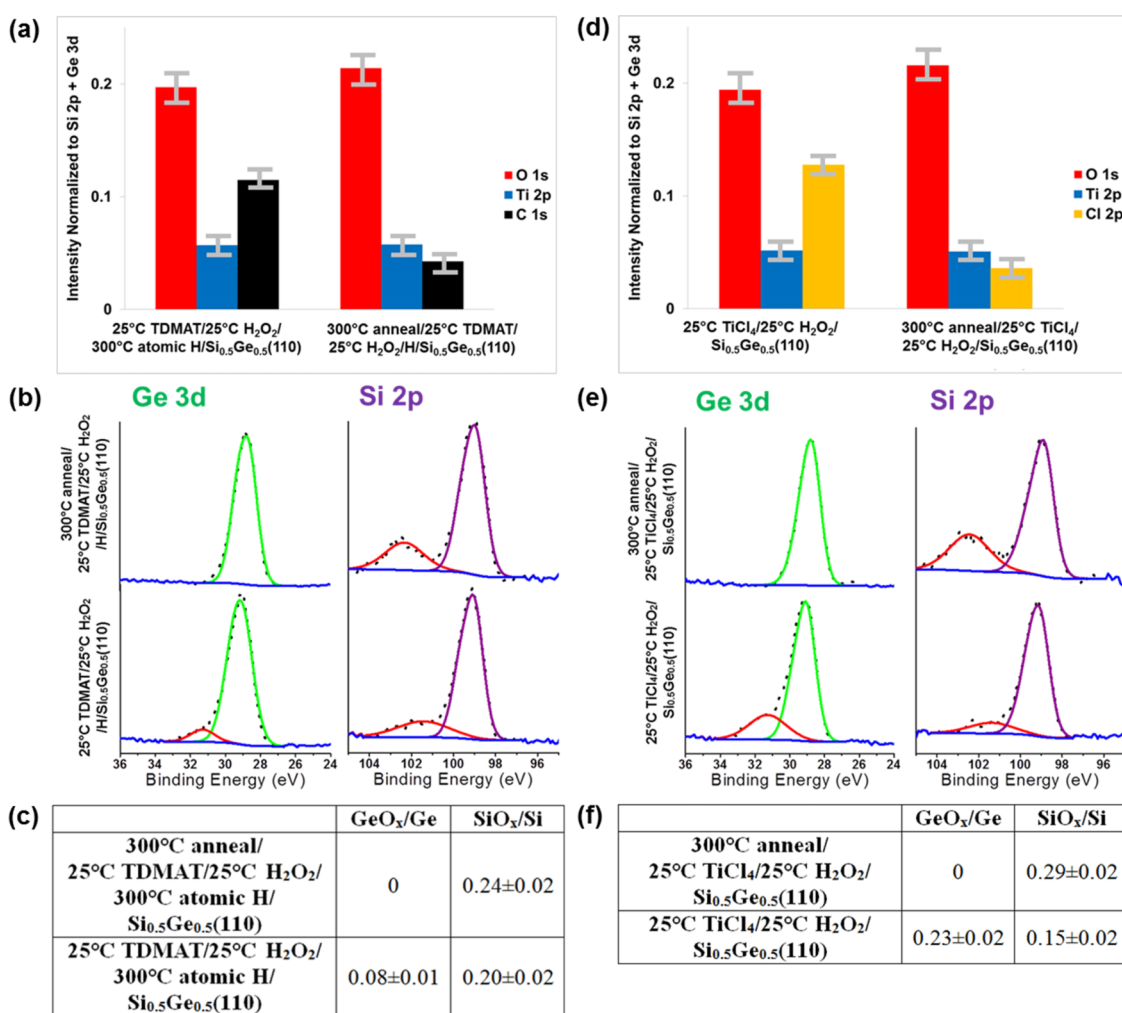


FIG. 3. XPS chemical compositions and Si 2p and Ge 3d spectra of TDMAT or TiCl_4 dosed $\text{Si}_{0.5}\text{Ge}_{0.5}(110)$ surfaces. (a) Chemical intensities normalized to Si 2p + Ge 3d peaks upon a 25 °C TDMAT dose. Ti:O:C ratios were 1:3:2 with error ranges of ± 0.02 and no N peak was observed. After 300 °C annealing, Ti and O ratios were constant consistent with a thermally stable TiO_x monolayer while C was decreased due to desorption of methanes or ethanes. (b) Ge 3d (green) and Si 2p (purple) peaks upon a 25 °C TDMAT dose followed by 300 °C PDA. After a TDMAT dose at 25 °C, XPS showed shoulder peaks (red) on both Ge 3d and Si 2p peaks corresponding to Ge—O—Ti and Si—O—Ti components. After annealing at 300 °C, Ge—O—Ti bonds disappeared and Si—O—Ti bonds increased. The shoulder peak of Si was shifted toward the higher binding energy by 1.0 eV after 300 °C PDA. (c) The table showed the ratios of GeO_x/Ge and SiO_x/Si with standard errors after 25 °C TDMAT dose and 300 °C PDA. 300 °C PDA removed GeO_x and increased SiO_x resulting in exclusively Si—O—Ti termination on $\text{Si}_{0.5}\text{Ge}_{0.5}(110)$. (d) Chemical intensities normalized to Si 2p + Ge 3d peaks upon a 25 °C TiCl_4 dose. Ti:O:Cl ratios were 1:3:2 and after 300 °C annealing, Ti and O ratios were constant while Cl was decreased by a $\text{HCl}(\text{g})$ desorption. These data were consistent with a thermally stable TiO_x monolayer while Cl was decreased due to the desorption of HCl . (e) XPS spectra upon a 25 °C TiCl_4 dose followed by 300 °C PDA. The change in shoulder peaks after 300 °C PDA was identical with (b). (f) The table shows the ratios of GeO_x/Ge and SiO_x/Si with standard errors after 25 °C TiCl_4 dose and 300 °C PDA. The surface was also composed of Si—O—Ti bonds after 300 °C PDA.

dose of TDMAT or TiCl_4 followed by 300 °C post-deposition annealing (PDA); the Ge 3d and Si 2p peaks are also presented. Based on the Hartree-Slater model,²⁸ all elemental intensities were corrected using photoelectron cross sections (Si 2p-0.817, Ge 3d-1.42, Ti 2p-7.81, O 1s-2.93, C 1s-1, Cl 2p-2.29) and normalized to the combination of Si 2p and Ge 3d peaks to estimate the ratios of each chemical component on the surfaces. As shown in Fig. 3(a), when 25 °C TDMAT was dosed onto 25 °C H_2O_2 /300 °C atomic H/ $\text{Si}_{0.5}\text{Ge}_{0.5}$ (110) surface, the ratios of Ti:O:C were 1:3:2 and no N signal was observed. In addition, the shoulder peaks of Si 2p and Ge 3d in Fig. 3(b) had the identical binding energies as those on the H_2O_2 dosed $\text{Si}_{0.5}\text{Ge}_{0.5}$ (110) surfaces (shown in Fig. S5 in the supplementary material); this demonstrated that Si—O—Ti and Ge—O—Ti bonds formed by H_2O_2 remained intact after low temperature TDMAT dosing.

After 300 °C PDA, the ratio of Ti and O remained constant demonstrating a thermally stable TiO_x monolayer while the C ratio was decreased. To explain these results, it was proposed that, upon annealing, Ti—O—Ti bonds were formed allowing C_2H_6 desorption. In addition, the shoulder peak of Si 2p was increased while the shoulder peak Ge 3d was disappeared consistent with the $\text{Si}_{0.5}\text{Ge}_{0.5}$ (110) surfaces being terminated with only Si—O—Ti bonds. It was expected that the thermal energy at 300 °C activated the Si atoms to diffuse to the top surface to bond with oxygen atoms and drove the Ge atoms to the subsurface due to the stronger bonds between Si and O compared to the bonds between Ge and O. Furthermore, the shoulder peak of Si 2p was shifted toward the higher binding by 1.0 eV after 300 °C PDA (between 101.5 and 102.5 eV) corresponding to Si^{3+} on 300 °C anneal/25 °C TDMAT/25 °C H_2O_2 /300 °C atomic H/ $\text{Si}_{0.5}\text{Ge}_{0.5}$ (110); this was consistent with the Si atoms making additional Si—O bonds upon annealing.

TiCl_4 , an inorganic precursor, was also dosed onto 25 °C H_2O_2 / $\text{Si}_{0.5}\text{Ge}_{0.5}$ (110) surface at 25 °C to provide a comparison between an inorganic precursor and TDMAT, an organometallic precursor. Fig. 3(d) showed that the ratios of Ti:O:Cl were 1:3:2 after a TiCl_4 dose at 25 °C on 25 °C H_2O_2 / $\text{Si}_{0.5}\text{Ge}_{0.5}$ (110) consistent with the results of TDMAT dosed 25 °C H_2O_2 /300 °C atomic H/ $\text{Si}_{0.5}\text{Ge}_{0.5}$ (110). Moreover, the shoulder peaks of Si 2p and Ge 3d in Fig. 3(e) had identical binding energies as 25 °C TDMAT/25 °C H_2O_2 /300 °C atomic H/ $\text{Si}_{0.5}\text{Ge}_{0.5}$ (110) in Fig. 3(c). This demonstrated that each Ti atom was likely to form Ti—O bonds by replacing two ligands with two oxygen atoms at the surface regardless of Ti precursors.

For the 25 °C TiCl_4 /25 °C H_2O_2 / $\text{Si}_{0.5}\text{Ge}_{0.5}$ (110), a subsequent PDA at 300 °C demonstrated that the monolayer of TiO_x was thermally stable as shown by the constant Ti and O ratios; however, the ratio of Cl was decreased due to the desorption of Cl_2 (g). In addition, as demonstrated in Fig. 3(e), the shoulder peaks of Si spectra showed a shift to higher binding energy while the shoulder peaks of Ge spectra were removed from the interface upon 300 °C PDA consistent with the results of 300 °C anneal/25 °C TDMAT/25 °C H_2O_2 /300 °C atomic H/ $\text{Si}_{0.5}\text{Ge}_{0.5}$ (110) in Fig. 3(b).

In Fig. 4, STS and XPS chemical shift measurements were performed to understand the electronic and chemical

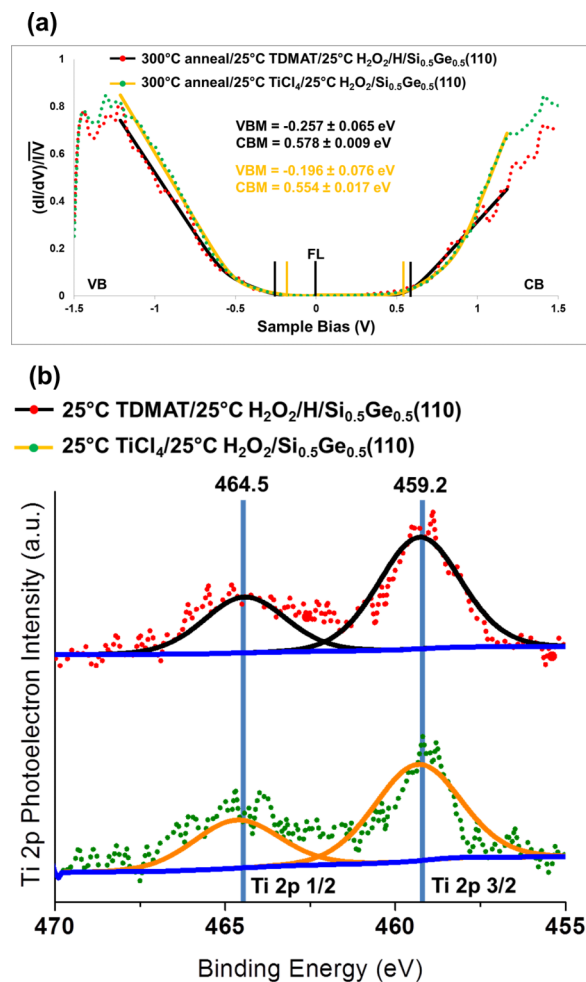


FIG. 4. STS measurements and Ti 2p peaks of TDMAT or TiCl_4 dosed $\text{Si}_{0.5}\text{Ge}_{0.5}$ (110) surfaces. (a) STS measurements of 300 °C anneal/25 °C TDMAT/25 °C H_2O_2 /300 °C atomic H/ $\text{Si}_{0.5}\text{Ge}_{0.5}$ (110) and 300 °C anneal/25 °C TiCl_4 /25 °C H_2O_2 / $\text{Si}_{0.5}\text{Ge}_{0.5}$ (110) surfaces. The Fermi level was positioned closer to VB edge on both surfaces consistent with the unpinning effect. Note: a bilinear fit was used for the VB side of the STS due to the band edge states. The reported VB positions are for the inner band gap. (b) Ti 2p peaks of TDMAT or TiCl_4 dosed $\text{Si}_{0.5}\text{Ge}_{0.5}$ (110). The Ti 2p 3/2 peaks on both surfaces were positioned at 459.2 eV corresponding to Ti^{4+} .

characteristics of a TiO_x monolayer on $\text{Si}_{0.5}\text{Ge}_{0.5}$ (110) surfaces. STS measurements in Fig. 4(a) verified identical electronic properties for 300 °C anneal/25 °C TDMAT/25 °C H_2O_2 /300 °C atomic H/ $\text{Si}_{0.5}\text{Ge}_{0.5}$ (110) (red) and 300 °C anneal/25 °C TiCl_4 /25 °C H_2O_2 / $\text{Si}_{0.5}\text{Ge}_{0.5}$ (110) (green) surfaces with ± 0.1 V difference near VB and CB edges. To achieve more accurate onsets near VB edges, the outer and inner VB edges were obtained from a bilinear fit; a bilinear fit was employed for these spectra since there were obvious band edge states. The bilinear fit of VB edge states results in calculation of two onsets. The two VB onsets were -0.578 ± 0.030 and -0.257 ± 0.065 V for 300 °C anneal/25 °C TDMAT/25 °C H_2O_2 /300 °C atomic H/ $\text{Si}_{0.5}\text{Ge}_{0.5}$ (110), and -0.513 ± 0.016 and -0.196 ± 0.076 V for 300 °C anneal/25 °C TiCl_4 /25 °C H_2O_2 / $\text{Si}_{0.5}\text{Ge}_{0.5}$ (110), respectively. Based on the results, it was concluded that a monolayer of TiO_x without mid-gap and CB edge states was formed on $\text{Si}_{0.5}\text{Ge}_{0.5}$ (110) surfaces using TDMAT or TiCl_4 . Additionally, compared to $\text{Si}_{0.5}\text{Ge}_{0.5}$ (110) surfaces

dosed with a 25 °C $\text{H}_2\text{O}_2(\text{g})$, the STS spectra after TDMAT or TiCl_4 dosing showed that state density near CB edge decreased; while consistent with the formation of a wide band monolayer of TiO_x , a detailed understanding of this change requires density functional theory (DFT) calculations. A bilinear fit was performed to determine the onset VB edges and the inner VB onsets were reported in Fig. 4(a). The increase in the bandgap after TiO_x formation is consistent with the formation for a wide bandgap TiO_x layer.

Fig. 4(b) presented XPS spectra of Ti 2p peaks on TDMAT or TiCl_4 dosed $\text{Si}_{0.5}\text{Ge}_{0.5}(110)$ surfaces to investigate the oxidation states. The positions of Ti 2p 3/2 and 1/2 spin-orbit components between two different $\text{Si}_{0.5}\text{Ge}_{0.5}(110)$ surfaces were almost the same with an error range of ± 0.1 eV. Furthermore, the positions of Ti 2p 3/2 peaks were located in 459.3 eV, and this binding energy corresponded to Ti^{4+} consistent with a proposed model of Ti atoms bonded to two O atoms with two other Ti—O or Ti—Cl bonds, which have stronger electronegativity than Ti atoms, as shown in detail below. Note that a pass energy of 50 eV was employed to achieve high intensity counts of the Ti 2p peak from a monolayer of TiO_x . This pass energy causes the broadening in the Ti 2p peak, and it was not possible to uniquely deconvolute the Ti 2p spectra into several distinct contributions. Therefore, it is possible that the broadening of the Ti 2p peak might be partially attributed to chemical states other than Ti^{4+} .

Proposed models of TDMAT or TiCl_4 dosed $\text{Si}_{0.5}\text{Ge}_{0.5}(110)$ surfaces followed by 300 °C PDA are shown

in Fig. 5. A proposed model in Fig. 5(a) shows that TDMAT molecules reacted with surface hydroxyl groups forming one Ti atom bonded to two oxygen atoms on $\text{Si}_{0.5}\text{Ge}_{0.5}(110)$ surface, two other ligands reacted with weakly bound hydroxyl groups from the surface forming two Ti—O—CH₃ bonds, and $\text{NH}(\text{CH}_3)_3$ or $\text{NH}_2(\text{CH}_3)_2$ desorbed as byproducts; note that it was proposed that the back bonded oxygens remained intact and this was consistent with the XPS peak intensities and shifts in Figs. 3 and 4. Moreover, a proposed model including Ti—O—CH₃ bonds was consistent with the previous report.²⁹ After 300 °C PDA, O=Ti—CH₃ bonds and additional Si—O—Si bonds were formed and $\text{C}_2\text{H}_6(\text{g})$ desorbs as a byproduct consistent with the XPS peak intensities and shifts; however, the experimental ratio between Ti:O was 1:3, while the proposed model in Fig. 3 had a Ti:O ratio of 1:5. In order to explain the ratio difference, a model must consider that many of oxygens are located at the subsurface and the emitted electrons should be affected by an exponential attenuation function according to the depth.³⁰ The electron escape depths for Ti and O peaks are 2 nm at normal incidence and decreased to 1 nm at 60° take-off angle,³⁰ which is the experimental condition during the XPS measurements. Based on the proposed model in which the depths of oxygen are assumed to be 0, 3, and 6 Å, a simple attenuation estimate using the electron escape depth of 1 nm provides a Ti and O ratio of 1:4, which is closer to the experimental results.

A model is also provided for the TiCl_4 reaction, as shown in Fig. 5(b), and TiCl_4 molecules reacted with hydroxyl

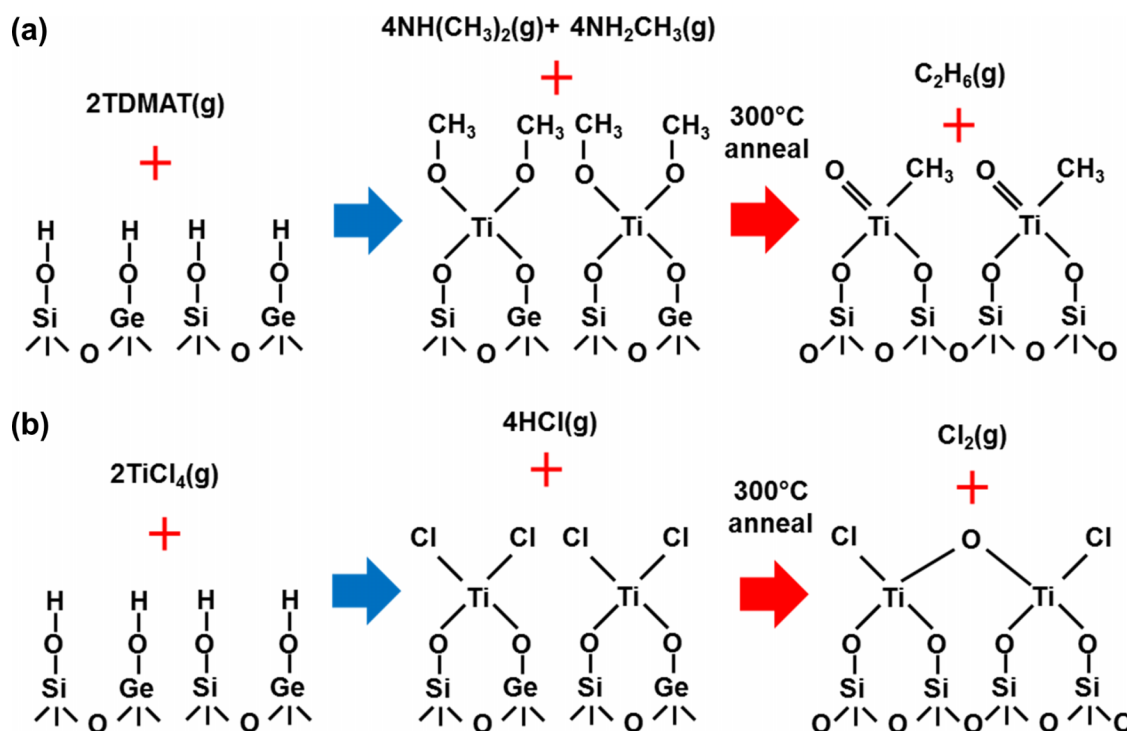


FIG. 5. Proposed models of TiCl_4 or TDMAT dosed $\text{H}_2\text{O}_2/\text{Si}_{0.5}\text{Ge}_{0.5}(110)$ surfaces. (a) A proposed model of the 25 °C TDMAT reaction + PDA. TDMAT molecules dissociatively chemisorbed to form one Ti atom bonded with two O atoms at the $\text{Si}_{0.5}\text{Ge}_{0.5}(110)$ surface along with two Ti—O—CH₃ bonds while $\text{NH}(\text{CH}_3)_3$ or $\text{NH}_2(\text{CH}_3)_2$ desorbed as byproducts. After 300 °C annealing, the model surface was composed of only Si—O—Ti and Si—O—Si bonds while ethane desorbed as a byproduct. (b) A proposed model of the 25 °C TiCl_4 reaction + PDA. TiCl_4 molecules were also likely to form one Ti atom bonded with two O atoms at the $\text{Si}_{0.5}\text{Ge}_{0.5}(110)$ surface while a byproduct desorbed as $\text{HCl}(\text{g})$. After 300 °C annealing, the model surface was composed of only Si—O—Ti and Si—O—Si bonds while Cl_2 desorbed as a byproduct; Ti—O—Ti bridge bonds formed to maintain the oxidation state (Ti^{4+}).

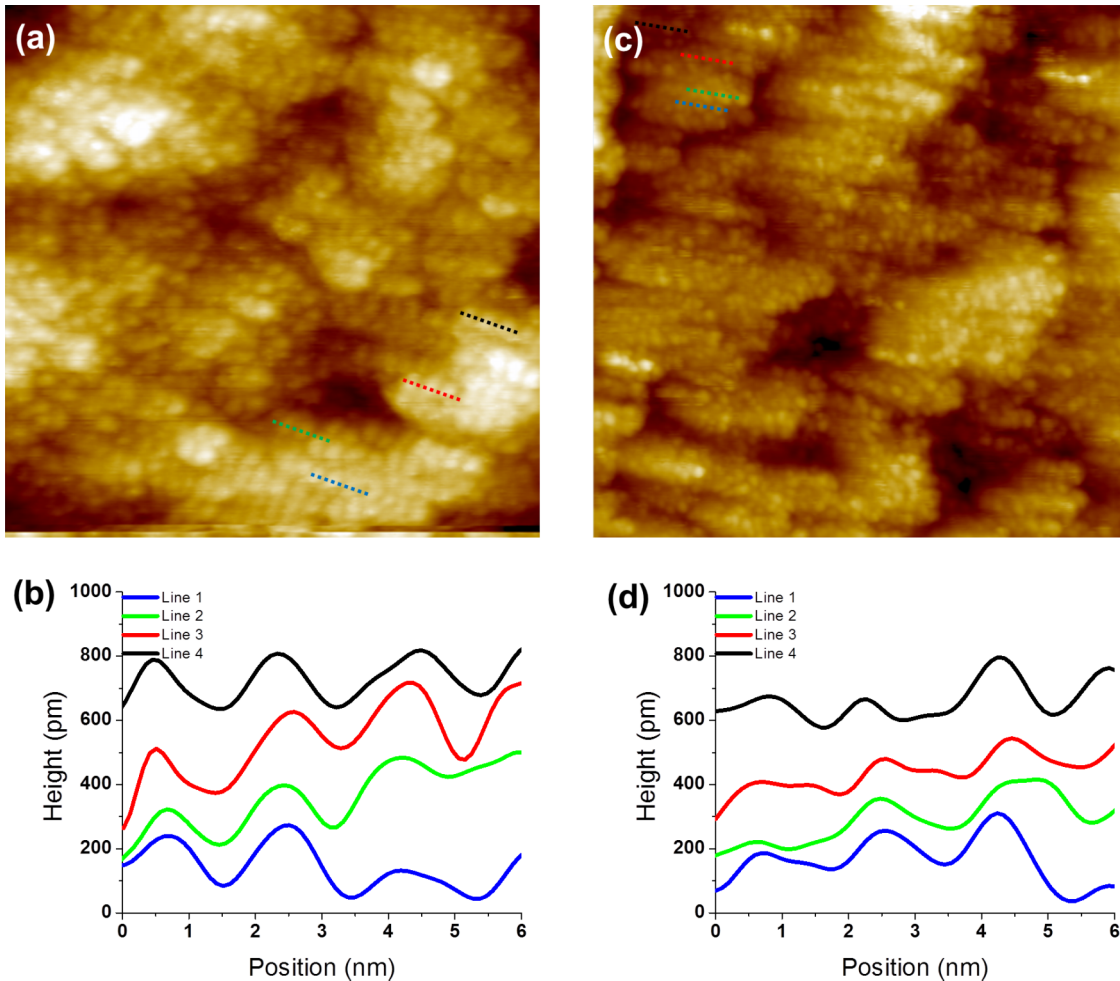


FIG. 6. STM images and line traces of TDMAT or TiCl_4 dosed $\text{Si}_{0.5}\text{Ge}_{0.5}(110)$ surfaces. (a) Filled state STM image ($50 \times 50 \text{ nm}^2$, $V_s = -1.8 \text{ V}$, $I_t = 200 \text{ pA}$) of $300 \text{ }^\circ\text{C}$ anneal/ $25 \text{ }^\circ\text{C}$ TDMAT/ $25 \text{ }^\circ\text{C}$ H_2O_2 / $300 \text{ }^\circ\text{C}$ atomic H/ $\text{Si}_{0.5}\text{Ge}_{0.5}(110)$ surface. (b) Line traces to estimate the row spacing in (a). The average row spacing was 18.0 \AA with a standard deviation of 1.7 \AA . (c) Filled state STM image ($50 \times 50 \text{ nm}^2$, $V_s = -1.8 \text{ V}$, $I_t = 200 \text{ pA}$) of $300 \text{ }^\circ\text{C}$ anneal/ $25 \text{ }^\circ\text{C}$ TiCl_4 / $25 \text{ }^\circ\text{C}$ CH_2O_2 / $\text{Si}_{0.5}\text{Ge}_{0.5}(110)$ surface. (d) Line traces to estimate the row spacing in (c). The average row spacing was 18.2 \AA with a standard deviation of 1.3 \AA .

groups resulting in the formation of one Ti atom bonded to two oxygen atoms on $\text{Si}_{0.5}\text{Ge}_{0.5}(110)$ surface while a $\text{HCl}(\text{g})$ desorbed as a byproduct. After $300 \text{ }^\circ\text{C}$ PDA, annealing induced the formation of Ti—O—Ti bonds allowing $\text{Cl}_2(\text{g})$ desorption and surface Si atoms formed additional Si—O backbonds. Note that proposed models were highly simplified to provide explanations with regard to the chemical compositions.

To compare the topology of $\text{Si}_{0.5}\text{Ge}_{0.5}(110)$ surfaces dosed with TDMAT or TiCl_4 followed by $300 \text{ }^\circ\text{C}$ PDA, STM images and line trace analyses are presented in Fig. 6. In Fig. 6(a), $300 \text{ }^\circ\text{C}$ anneal/ $25 \text{ }^\circ\text{C}$ TDMAT/ $25 \text{ }^\circ\text{C}$ H_2O_2 / $300 \text{ }^\circ\text{C}$ atomic H/ $\text{Si}_{0.5}\text{Ge}_{0.5}(110)$ surface showed consistent vertical rows. To analyze the row spacing, four different areas in the STM image were analyzed and line traces were performed as shown in Fig. 6(b). Line traces of $300 \text{ }^\circ\text{C}$ anneal/ $25 \text{ }^\circ\text{C}$ TDMAT/ $25 \text{ }^\circ\text{C}$ H_2O_2 / $300 \text{ }^\circ\text{C}$ atomic H/ $\text{Si}_{0.5}\text{Ge}_{0.5}(110)$ surface showed an average row spacing of 18.0 \AA with a standard deviation of 1.7 \AA and a standard error of 0.60 \AA . This row spacing was more than twice the 8.0 \AA of adatom spacing on a sputter-cleaned $\text{Si}_{0.5}\text{Ge}_{0.5}(110)$ surface consistent with the proposed models in Fig. 5(a), in which one Ti atom is bonded to two oxygen atoms on

$\text{Si}_{0.5}\text{Ge}_{0.5}(110)$ surface with the oxygen backbond insertion. In comparison, Fig. 6(c) shows the STM image of $300 \text{ }^\circ\text{C}$ anneal/ $25 \text{ }^\circ\text{C}$ TiCl_4 / $25 \text{ }^\circ\text{C}$ H_2O_2 / $\text{Si}_{0.5}\text{Ge}_{0.5}(110)$ surface. The line traces in Fig. 6(d) show an average row spacing of 18.2 \AA with a standard deviation of 1.3 \AA and a standard error of 0.47 \AA . Therefore, there is an identical row spacing for TDMAT and TiCl_4 dosing followed by PDA within an error range demonstrated the formation of TiO_x monolayer with the same surface structure independent of precursors. Compared to the 11.8 \AA average row spacing of a monolayer of Al_2O_3 on $\text{Si}_{0.5}\text{Ge}_{0.5}(110)$ surface, in which one Al atom was bonded to one oxygen atom with the ratio of Al:O to be 2:3 on $\text{Si}_{0.5}\text{Ge}_{0.5}(110)$,¹⁴ the TiO_x row spacing was larger as shown in the proposed model in Figs. 5(a) and 5(b) for Ti making two bonds to surface O atoms.

IV. CONCLUSIONS

Clean or H-terminated $\text{Si}_{0.5}\text{Ge}_{0.5}(110)$ surfaces were dosed with $\text{H}_2\text{O}_2(\text{g})$ at $25 \text{ }^\circ\text{C}$ to functionalize the surfaces with hydroxyls. STS measurements demonstrated that $\text{H}_2\text{O}_2(\text{g})$ resulted in the identical electronic and $-\text{OH}$ terminated

molecular structures on both clean and H-terminated $\text{Si}_{0.5}\text{Ge}_{0.5}(110)$ surfaces. To form a monolayer of TiO_x on hydroxyl-terminated $\text{Si}_{0.5}\text{Ge}_{0.5}(110)$ surfaces, TDMAT or TiCl_4 were subsequently dosed at 25°C on 25°C $\text{H}_2\text{O}_2/300^\circ\text{C}$ atomic H/ $\text{Si}_{0.5}\text{Ge}_{0.5}(110)$ and 25°C $\text{H}_2\text{O}_2/\text{Si}_{0.5}\text{Ge}_{0.5}(001)$ surfaces. XPS indicated that the ratio between Ti and O was 1:3 and remained constant upon 300°C PDA demonstrating a thermally stable monolayer of TiO_x regardless of Ti-based precursors. STM images showed that the row spacing of TiO_x monolayer on $\text{Si}_{0.5}\text{Ge}_{0.5}(110)$ surfaces was more than twice the adatom spacing on a clean $\text{Si}_{0.5}\text{Ge}_{0.5}(110)$ verifying a proposed chemisorption model. XPS analysis verified that a monolayer of TiO_x was composed of only Si—O—Ti bonds after PDA indicating the complete segregation of Si atoms. Furthermore, STS measurements were consistent with the monolayer of TiO_x having no mid-gap and CB edge states, which should be an ideal ultrathin insulating layer for a MIS structure.

SUPPLEMENTARY MATERIAL

See [supplementary material](#) for the properties of $\text{Si}_{0.5}\text{Ge}_{0.5}(110)$ surfaces.

ACKNOWLEDGMENTS

This work was supported in part by the Center for Low Energy Systems Technology (LEAST), one of the six centers of STARnet, a Semiconductor Research Corporation program (Grant No. 2013-VJ-2451) sponsored by MARCO and DARPA, NSF DMR 1207213, GLOBALFOUNDRIES, and Applied Materials. The $\text{Si}_{0.5}\text{Ge}_{0.5}$ wafers were provided by GLOBALFOUNDRIES.

¹F. Schaffler, *Semicond. Sci. Technol.* **12**, 1515 (1997).

²D. J. Paul, *Semicond. Sci. Technol.* **19**, R75 (2004).

³M. L. Lee, E. A. Fitzgerald, M. T. Bulsara, M. T. Currie, and A. Lochtefeld, *J. Appl. Phys.* **97**, 011101 (2005).

⁴B. G. Streetman and S. Banerjee, *Solid State Electronic Devices*, 6th ed. (Pearson Prentice Hall, Upper Saddle River, NJ, 2006).

⁵M. Lundstrom, *Fundamentals of Carrier Transport*, 2nd ed. (Cambridge University Press, Cambridge, UK, New York, 2000).

⁶M. L. Lee, C. W. Leitz, Z. Cheng, A. J. Pitera, T. Langdo, M. T. Currie, G. Taraschi, E. A. Fitzgerald, and D. A. Antoniadis, *Appl. Phys. Lett.* **79**, 3344 (2001).

⁷T. Ghani, M. Armstrong, C. Auth, M. Bost, P. Charvat, G. Glass, T. Hoffmann, K. Johnson, C. Kenyon, J. Klaus, B. McIntyre, K. Mistry, A. Murthy, J. Sandford, M. Silberstein, S. Sivakumar, P. Smith, K. Zawadzki, S. Thompson, and M. Bohr, "A 90nm high volume manufacturing logic technology featuring novel 45nm gate length strained silicon CMOS transistors," in *IEEE International Electron Devices Meeting 2003 (IEEE, 2003)*, p. 11.6.1.

⁸S. Verdonckt-Vandebroek, E. F. Crabbe, B. S. Meyerson, D. L. Harame, P. J. Restle, J. M. C. Stork, and J. B. Johnson, *IEEE Trans. Electron Devices* **41**, 90 (1994).

⁹J. P. Snyder, C. R. Helms, and Y. Nishi, *Appl. Phys. Lett.* **67**, 1420 (1995).

¹⁰D. Kuzum, T. Krishnamohan, A. J. Pette, A. K. Okyay, Y. Oshima, Y. Sun, J. P. McVittie, P. A. Pianetta, P. C. McIntyre, and K. C. Saraswat, *IEEE Electron Device Lett.* **29**, 328 (2008).

¹¹J. S. Lee, T. Kaufman-Osborn, W. Melitz, S. Lee, and A. Kummel, *Surf. Sci.* **605**, 1583 (2011).

¹²T. Kaufman-Osborn, E. A. Chagarov, and A. C. Kummel, *J. Chem. Phys.* **140**, 204708 (2014).

¹³T. Kaufman-Osborn, E. A. Chagarov, S. W. Park, B. Sahu, S. Siddiqui, and A. C. Kummel, *Surf. Sci.* **630**, 273 (2014).

¹⁴S. W. Park, H. Kim, E. Chagarov, S. Siddiqui, B. Sahu, N. Yoshida, J. Kachian, R. Feenstra, and A. C. Kummel, *Surf. Sci.* **652**, 322 (2016).

¹⁵M. Kobayashi, A. Kinoshita, K. Saraswat, H.-S. P. Wong, and Y. Nishi, *J. Appl. Phys.* **105**, 023702 (2009).

¹⁶R. R. Lieten, S. Degroote, M. Kuijk, and G. Borghs, *Appl. Phys. Lett.* **92**, 022106 (2008).

¹⁷J.-Y. J. Lin, A. M. Roy, A. Nainani, Y. Sun, and K. C. Saraswat, *Appl. Phys. Lett.* **98**, 092113 (2011).

¹⁸S. Chakraborty, M. K. Bera, P. K. Bose, and C. K. Maiti, *Semicond. Sci. Technol.* **21**, 335 (2006).

¹⁹S. L. Manatt and M. R. R. Manatt, *Chem. - Eur. J.* **10**, 6540 (2004).

²⁰R. M. Feenstra, J. A. Stroscio, and A. P. Fein, *Surf. Sci.* **181**, 295 (1987).

²¹R. M. Feenstra, *Surf. Sci.* **299–300**, 965 (1994).

²²R. M. Feenstra, J. Y. Lee, M. H. Kang, G. Meyer, and K. H. Rieder, *Phys. Rev. B* **73**, 035310 (2006).

²³R. M. Feenstra, *Phys. Rev. B* **50**, 4561 (1994).

²⁴Y. Sun, Z. Liu, S. Y. Sun, and P. Pianetta, *J. Vac. Sci. Technol. A* **26**, 1248 (2008).

²⁵Y. J. Chabal, G. S. Higashi, K. Raghavachari, and V. A. Burrows, *J. Vac. Sci. Technol. A* **7**, 2104 (1989).

²⁶X. Zhang, E. Garfunkel, Y. J. Chabal, S. B. Christman, and E. E. Chaban, *Appl. Phys. Lett.* **79**, 4051 (2001).

²⁷S. Rivillon, Y. J. Chabal, F. Amy, and A. Kahn, *Appl. Phys. Lett.* **87**, 2531011 (2005).

²⁸J. H. Scofield, *J. Electron Spectrosc. Relat. Phenom.* **8**, 129 (1976).

²⁹F. Bini, C. Rosier, R. P. Saint-Arroman, E. Neumann, C. Dablemont, A. de Mallmann, F. Lefebvre, G. P. Niccolai, J.-M. Basset, M. Crocker, and J.-K. Buijink, *Organometallics* **25**, 3743 (2006).

³⁰*Practical Surface Analysis, Auger and X-ray Photoelectron Spectroscopy*, edited by D. Briggs and M. P. Seah (John Wiley & Sons, Chichester, 1983).